Biomaterials 182 (2018) 157–166

Contents lists available at ScienceDirect

Biomaterials

journal homepage: www.elsevier.com/locate/biomaterials

PEGylated tumor cell membrane vesicles as a new vaccine platform for cancer immunotherapy

Lukasz J. Ochyl[a,b], Joseph D. Bazzill[a,b], Charles Park[b,c], Yao Xu[a,b], Rui Kuai[a,b], James J. Moon[a,b,c,*]

[a] Department of Pharmaceutical Sciences, University of Michigan, Ann Arbor, MI 48109, USA
[b] Biointerfaces Institute, University of Michigan, Ann Arbor, MI 48109, USA
[c] Department of Biomedical Engineering, University of Michigan, Ann Arbor, MI 48109, USA

A B S T R A C T

Despite the promise and advantages of autologous cancer cell vaccination, it remains challenging to induce potent anti-tumor immune responses with traditional immunization strategies with whole tumor cell lysate. In this study, we sought to develop a simple and effective approach for therapeutic vaccination with autologous whole tumor cell lysate. Endogenous cell membranes harvested from cancer cells were formed into PEGylated nano-vesicles (PEG-NPs). PEG-NPs exhibited good serum stability *in vitro* and draining efficiency to local lymph nodes upon subcutaneous administration *in vivo*. Vaccination with PEG-NPs synthesized from murine melanoma cells elicited 3.7-fold greater antigen-specific cytotoxic $CD8^+$ T lymphocyte responses, compared with standard vaccination with freeze-thawed lysate in tumor-bearing mice. Importantly, in combination with anti-programmed death-1 (αPD-1) IgG immunotherapy, PEG-NP vaccination induced 4.2-fold higher frequency of antigen-specific T cell responses ($P < 0.0001$) and mediated complete tumor regression in 63% of tumor-bearing animals ($P < 0.01$), compared with FT lysate + αPD-1 treatment that exhibited only 13% response rate. In addition, PEG-NPs + αPD-1 IgG combination immunotherapy protected all survivors against a subsequent tumor cell re-challenge. These results demonstrate a general strategy for eliciting anti-tumor immunity using endogenous cancer cell membranes formulated into stable vaccine nanoparticles.

1. Introduction

Cancer is a continually increasing concern facing the aging population, and the rising incidence of melanoma of the skin leads to nearly 100,000 new cases and over 9000 deaths per year in the US [1]. The immunotherapy breakthroughs over the past decade have recognized the previously suggested role of the immune system in fighting cancer, leading to the clinical approval of checkpoint blockade inhibitors, including αCTLA-4 and αPD-1 antibodies [2–4]. While tumor regression and complete cures have been seen with these approaches in many patients, the limited response rate to immune checkpoint blockade demonstrates the need for new complementary approaches [5].

One of the drawbacks of PD-1 targeting is the reliance on patients' endogenous tumor-specific cytotoxic T lymphocyte (CTL) responses, which may be low or absent [6]. Therapeutic vaccination may address this issue by eliciting CTL responses, but current cancer vaccine approaches require identification and manufacturing of tumor antigens [7,8]. Specifically, following tumor exome sequencing, peptide- or mRNA-based neo-antigen vaccines have been shown to deliver large doses of immunogenic epitopes, resulting in strong and durable responses [9–12]. In contrast, tumor cell lysate, which contains patient's own library of tumor-associated and tumor-specific antigens, is readily available for processing into vaccines without the need for sequencing or antigen synthesis [13]. However, vaccination with tumor cell lysate induces weak anti-tumor T-cell responses with limited therapeutic efficacy [14–16]. To address this, nanoparticles or dendritic cell-based vaccines have been utilized, but it has been challenging to achieve potent CTL responses with therapeutic efficacy using tumor cell lysate [17–21].

In this study, we report a simple method for generating vaccine nanoparticles from tumor cell lysate and demonstrate their ability to elicit strong T-cell responses with potent therapeutic efficacy. Exploiting the recent advances in plasma membrane-based drug delivery approaches, including vaccines [22–26], we formulated tumor cell membranes into monodisperse nanoparticles coated with a surface layer of polyethylene glycol (PEG-NPs) (Fig. 1). We report that PEG-NPs exhibited enhanced serum stability and efficiently trafficked to local lymph nodes (LNs), resulting in enhanced T cell responses and anti-tumor activity. The combination of PEG-NPs vaccination and αPD-1 antibody immunotherapy led to complete tumor regression in 63% of animals and established protective immunity against future tumor re-challenge. These data demonstrate that tumor cell membrane formulated into stable PEGylated nanoparticles can serve as a potent cancer vaccine platform.

* Corresponding author. Department of Pharmaceutical Sciences, University of Michigan, Ann Arbor, MI 48109, USA.
E-mail address: moonjj@umich.edu (J.J. Moon).

https://doi.org/10.1016/j.biomaterials.2018.08.016
Received 6 May 2018; Received in revised form 1 August 2018; Accepted 6 August 2018
Available online 09 August 2018
0142-9612/

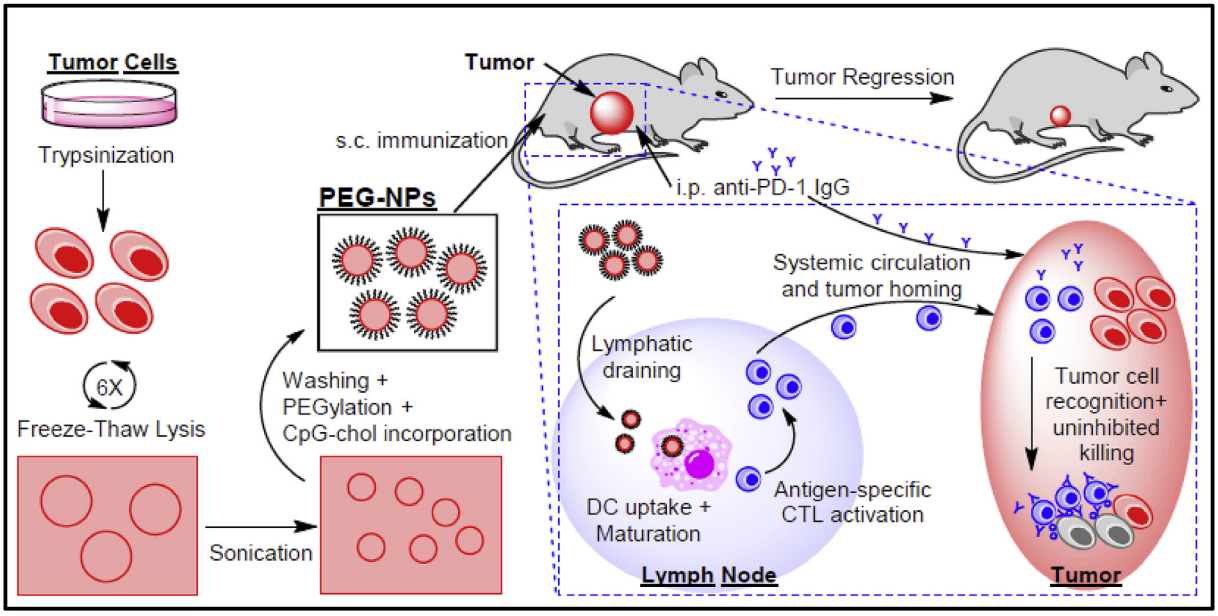

Fig. 1. Schematic representation of PEG-NPs preparation and therapy. B16F10 OVA cells are lysed via freeze-thaw cycling, sonicated to form nano-sized vesicles, collected after calcium-mediated aggregation, and washed. PEGylation, removal of calcium with EDTA, and further wash steps are then performed. Finally, cholesterol-linked CpG is incorporated, resulting in the formation of PEG-NPs. Upon subcutaneous administration in tumor-bearing mice, PEG-NPs drain efficiently to lymph nodes (LNs) where they are taken up by DCs for activation of antigen-specific cytotoxic $CD8^+$ T lymphocytes (CTLs). After tumor-infiltration, CTLs recognize and kill cancer cells in synergy with *anti*-PD-1 immune checkpoint blockade, leading to tumor regression.

2. Materials and methods

2.1. Cell culture

B16F10 OVA cells, expressing an exogenous model antigen, OVA, with a transmembrane domain, were grown in RPMI 1640 media supplemented with 10% FBS, 100 U/mL penicillin, and 100 μg/mL streptomycin. B16F10 OVA cells were kindly provided by the lab of Prof. Darrell Irvine (Massachusetts Institute of Technology; Cambridge, MA). Bone marrow-derived dendritic cells (BMDCs) were cultured as previously described [27]. Briefly, tibiae and femurs of C57BL/6 mice (Envigo) were harvested and the bone marrow extracted by flushing media through the bones using a syringe equipped with a 26 gauge needle. Cells were passed through a 40 μm strainer to remove debris, washed, and plated. Complete media (RPMI supplemented on 10% FBS, 100 U/mL penicillin, 100 μg/mL streptomycin, 50 μM β-mercaptoethanol, and 20 ng/mL GM-CSF) was supplemented on day 3 and refreshed on days 6, 8, and 10. BMDCs were used on days 8–12 from the suspended and loosely-adhered cell population.

2.2. Preparation of tumor cell lysate

Tissue culture-grown B16F10 OVA cells were trypsinized and washed three times with PBS. Cells were resuspended at 1×10^8 cells/mL and lysed by freeze-thaw cycling (10 min in liquid nitrogen and 10 min in 37 °C water bath; 6 cycles total). Low-speed centrifugation (100 × g, 10 min) was used to remove large debris and generate freeze-thaw lysate from the supernatant. Sonicated lysate was obtained by probe-tip sonicating FT lysate for 2 min on ice using 50% intensity setting (QSonica, 125 W/20 kHz sonicator) and collecting the supernatant after centrifugation (10,000 × g, 10 min). Cytosol and membrane fractions were generated by ultracentrifugation (200,000 × g, 1 h) of sonicated lysate and collecting the supernatant and pellet, respectively.

2.3. Preparation of PEG-NPs

To generate PEGylated tumor cell membrane nanoparticles, we first sonicated FT lysate (6 mg/mL) in PBS as above and then induced aggregation of membrane vesicles by adding 20 mM $CaCl_2$, followed by incubation at 37 °C for 1 h. The resulting cell membrane particles were washed two times with PBS via centrifugation (20,000 × g, 5 min) and resuspended in PBS containing 100 mM EDTA and 10 mg/mL methoxy-poly (ethylene glycol) - 1, 2-distearoyl-*sn*-glycero-3-phosphoethanolamine-N (DSPE-PEG, 5 kDa average molecular weight; Laysan Bio, Inc.). Aggregates were fully dispersed after 1 min of water-bath sonication and then incubated for 1 h at 37 °C to allow post-insertion of DSPE-PEG. For preparation of unPEGylated nanoparticles (NPs) PBS solution containing 100 mM EDTA omitting DSPE-PEG was used for the final incubation. The resulting PEG-NPs were purified by passing through Zeba desalting column (7 K molecular weight cut-off, Thermo Fisher Scientific).

2.4. Characterization of tumor cell lysate and PEG-NPs

Sample concentrations for all assays were standardized by the total protein content as measured by MicroBCA Assay Kit (Thermo Scientific). SDS-PAGE was performed, followed by gel staining with Coomassie or transfer to a PVDF membrane for Western Blotting using antibodies against gp100 (Abcam), TRP2 (Santa Cruz), or ovalbumin (Abcam). Transmission electron microscopy images were obtained using JEOL 1400-plus microscope (JOEL USA) following sodium phosphotungstate negative staining. Particle size and zeta potential were measured and analyzed using dynamic light scattering (DLS, Malvern Zetasizer Nano Range) in PBS or ultrapure water, respectively. For stability studies, samples were incubated with PBS or 10% FBS in PBS at 4 °C (long term) or at 37 °C while shaking (short term) as indicated in the figures.

2.5. Protein uptake by dendritic cells

In order to obtain fluorescently labeled lysate, trypsinized B16F10 OVA cells (2 million cells/mL) were incubated with 1 μM Oregon Green 488 carboxylic acid, succinimidyl ester (OG488, Thermo Fisher Scientific) in RPMI at 37 °C for 10 min. Lysate was prepared as

described above and then incubated with BMDCs for 24 h. Cells were then washed, trypsinized, and resuspended in FACS buffer (1% BSA in PBS) containing anti-CD16/32 blocking antibodies. Cells were stained with CD11c antibody, washed, and analyzed via flow cytometry for OG488 signal.

2.6. T cell expansion

In vitro T cell expansion was examined by pulsing BMDCs (50,000 cells per well) overnight with lysate fractions or PEG-NPs at 1 mg/mL in 96-well plates. As indicated, 5 μg/mL CpG (IDT) or 1 μg/mL MPLA (Avanti Polar Lipids) was used as adjuvants. BMDCs were washed three times with PBS. Harvested OT-I transgenic $CD8^+$ T cells purified from spleens using a negative selection kit (Stemcell Technologies) were labeled with CFSE (1 μM concentration, 2 million cells/mL, 10 min in RPMI), washed, and added to BMDC-containing wells. After three days of co-incubation the cells were collected by pipetting, blocked with FACS buffer containing anti-CD16/32 antibodies, stained with anti-CD8α and live/dead marker, washed, and analyzed via flow cytometry. T cell expansion and viability were analyzed using dilution of the CFSE signal and count of surviving live T cells ($DAPI^-/CD8\alpha^+$), respectively. Proliferation Index was calculated using Proliferation Platform in FlowJo.

2.7. Lymph node draining

B16F10 OVA cell membranes were labeled with lipophilic DiD dye (1,1′-Dioctadecyl-3,3,3′,3′-Tetramethylindodicarbocyanine) by incubating 5 million cells/mL at 37 °C for 10 min with 1 μg/mL DiD. Cells were washed three times with PBS to remove any unincorporated dye and processed into fractions and NPs as described above. Labeled formulations were normalized by DiD fluorescence and administered subcutaneously at the tail base of C57BL/6 mice (n = 4). Mice were euthanized either 4, 24, or 48 after injection, and inguinal LNs were harvested and imaged using *In Vivo* Imaging System (IVIS) to assess radiance efficiency. Then, LNs were processed into single cell suspensions using a 40 μm cell strainer, washed, and blocked with FACS buffer containing anti-CD16/32 blocking antibodies. Next, we stained the cells for markers of macrophages (*anti*-F4/80 antibody), B cells (B220), and DCs (anti-CD11c antibody), washed the cells, and analyzed with flow cytometry.

2.8. Animal experiments

All immunizations and tumor studies were performed according to the federal, state, and local guidelines. All work performed on animals was in accordance with and approved by University Committee on Use and Care of Animals (UCUCA) at the University of Michigan, Ann Arbor. For all immunizations, cholesterol-modified CpG (IDT) was incubated with vaccine formulations at 37 °C for 30 min prior to administration. For the prophylactic vaccination studies, 6–8 weeks old, female C57BL/6 mice were immunized subcutaneously at the tail base with 1 mg of total protein and 15 μg of CpG on days 0 and 14, followed by a challenge with 1×10^6 B16F10 OVA cells injected s.c. at the flank on day 35. For the therapeutic vaccination studies, 6–8 weeks old, female C57BL/6 mice were inoculated with 2×10^5 B16F10 OVA cells s.c. at the flank on day 0, and immunized with vaccine formulations (1 mg of total protein and 15 μg of CpG) on days 5 and 12 with or without co-administration of *anti*-PD-1 IgG (i.p.; 100 μg per mouse per injection) on days 6, 9, 13, and 16. Tumor size was measured every other day and the volume determined using the following formula: $0.5 \times \text{length} \times \text{width}^2$.

2.9. Tetramer staining

Cytotoxic T lymphocyte responses were analyzed by tetramer staining one week after each immunization as described before [28]. Briefly, 150 μL of blood was collected and red blood cells were removed with ACK lysis buffer. Peripheral blood mononuclear cells (PBMCs) were washed, blocked with FACS buffer containing anti-CD16/32 blocking antibodies, and stained with H-2Kb OVA Tetramer-SIINFEKL-PE (MBL International), followed by staining with anti-CD8 antibody. Cells were washed, dead cells were labeled with DAPI, and the final suspension analyzed by flow cytometry.

2.10. Statistical analyses

For animal studies, mice were randomized to match average volumes of the primary tumors, and all procedures were performed in a non-blinded fashion. Statistical analysis was performed with Prism 6.0 software (GraphPad Software) by one-way or two-way ANOVA with Tukey's comparisons post-test, as indicated. Statistical significance for survival curve was calculated by the log-rank test. Statistical significance is indicated as $^*P < 0.05$, $^{**}P < 0.01$, $^{***}P < 0.001$, and $^{****}P < 0.0001$.

3. Results and discussion

3.1. Characterization of tumor cell lysate

In this study, we aimed to use tumor cell lysate to generate adaptive anti-tumor immune responses, and we have utilized B16F10 OVA murine melanoma cells expressing a model antigen ovalbumin (OVA) on their plasma membrane. We generated sonicated cell lysate by freeze-thaw cycles, followed by probe-tip sonication and centrifugation to remove large debris (Fig. 1). Examination of cell lysate under transmission electron microscopy demonstrated the presence of nano-sized structures (Fig. 2A), which we suspected to be self-assembled remnants of the plasma membrane. The membrane fraction was separated via ultracentrifugation and demonstrated to contain various proteins as shown by gel electrophoresis (Fig. 2B). We performed Western blotting to test for the retention of tumor-associated antigens in the membrane fraction. Proteins with a transmembrane domain, such as endogenous glycoprotein 100 (gp100) and tyrosine-related protein 2 (TRP2) [29,30], along with the model antigen OVA (a transmembrane protein in our B16F10 OVA cell line) were detected in varying levels in either the whole cell lysate or the membrane fraction (lane 1 and 2, respectively; Fig. 2B).

When incubated with BMDCs *in vitro*, membrane-associated proteins were preferentially taken up by DCs ($P < 0.0001$, Fig. 2C), in contrast to inefficient uptake of cytosolic proteins by DCs. This suggests that proteins associated with membrane vesicles have increased interactions with antigen-presenting cells (APCs), leading to enhanced phagocytosis of cellular proteins. We hypothesized that this enhanced uptake and eventual presentation of antigens in the context of major histocompatibility complex-I (MHC-I) would result in activation of antigen-specific CTLs. To test this, we isolated OVA-specific CD8α+ T cells from OT-I transgenic mice, co-cultured them with lysate-pulsed BMDCs, and examined proliferation of OT-I CD8α+ T cells. The cell membrane fraction, characterized by enhanced DC uptake and high antigen content, led to significantly increased T cell expansion *in vitro* ($P < 0.001$, Fig. 2D), compared with the cytosolic or whole lysate fractions. To further potentiate T cell expansion each group was tested with the addition of an immunostimulatory agent, monophosphoryl lipid A (MPLA, a Toll-like receptor-4 agonist). A similar trend of T cell expansion was observed after addition of MPLA, with the membrane fraction generating the greatest extent of CD8α+ T cell proliferation among all the groups ($P < 0.001$, Fig. 2D). These results showed that the membrane fraction of cell lysate contained vesicular nanostructures with tumor-associated antigens and that DCs pulsed with these membrane vesicles primed antigen-specific CD8α+ T cell responses *in vitro*.

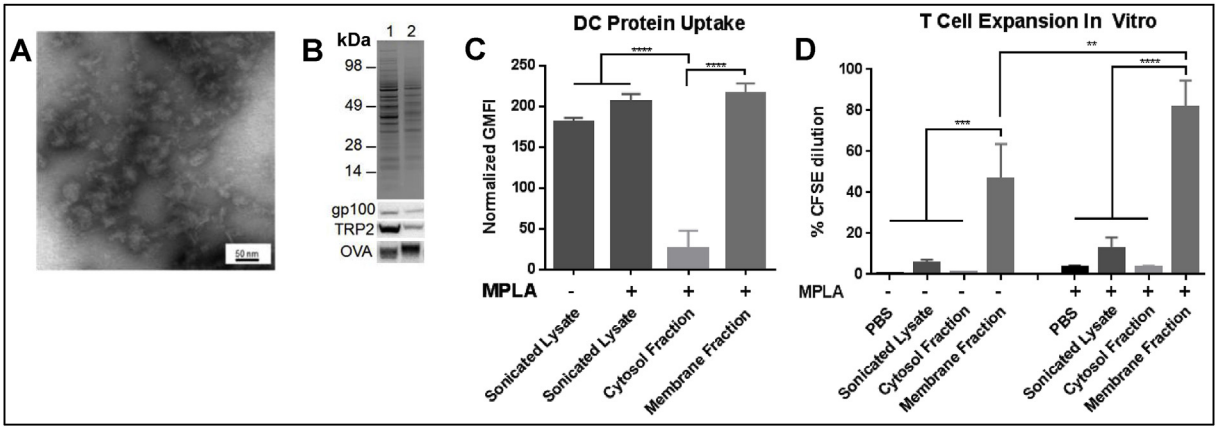

Fig. 2. Characterization of membrane fraction of tumor cell lysate. A. TEM image of cell lysate shows nano-sized membrane structures. **B.** Wide protein repertoire from whole cell lysate (lane 1) is retained within the membrane fraction (lane 2) as seen via Coomassie staining (top panel). Tumor-associated antigens (gp100 and TRP2) and model antigen (OVA) incorporation was determined by Western Blot analysis (bottom three panels). **C.** Fluorophore-labeled lysate, cytosol fraction, and membrane fraction were pulsed to dendritic cells, and the relative protein uptake was analyzed by flow cytometry. **D.** Dendritic cells were pulsed with lysate fractions with or without MPLA and co-cultured with OT-I OVA-specific $CD8^+$ T cells. T cell proliferation was measured by the dilution of CFSE dye via flow cytometry. Mean ± SD are shown. Statistical analysis was performed using two-way ANOVA comparison with Tukey's multiple comparison test (**$P < 0.01$, ***$P < 0.001$, ****$P < 0.0001$).

3.2. Preparation and characterization of PEG-NPs

Having shown induction of CD8α+ T cells with membrane vesicles *in vitro*, we sought to further characterize them along the preparation procedure and improve their overall stability for the subsequent vaccination studies *in vivo* (see below). When B16F10 OVA cells were harvested and cycled between liquid nitrogen and 37 °C water bath, followed by low speed centrifugation, the resulting supernatant contained large, poly-disperse structures, which we termed freeze-thawed (FT) lysate. Analyses with dynamic light scattering indicated that FT lysate contained vesicles with an average hydrodynamic diameter of 610 ± 60 nm, a polydispersity index (PDI) of 0.67 ± 0.12, and zeta potential of −30 mV ± 1 mV (Fig. 3A). Further probe-tip sonication and removal of large debris via high speed centrifugation yielded smaller and monodisperse membrane vesicles with 180 ± 2 nm hydrodynamic diameter, PDI of 0.28 ± 0.02, and zeta potential of −25 mV ± 1 mV (Fig. 3A).

We examined the stability of FT lysate stored at 4 °C in PBS or 10% FBS-containing PBS for approximately one month. Under either condition, FT lysate vesicles increased in size to approximately 1 μm, and PDI values increased beyond 0.70 (Fig. 3B). Endogenous nano-vesicles present in the sonicated lysate preparation (without PEGylation) also aggregated over the four-week period in PBS, increasing in size from 180 nm to 280 nm and becoming more polydisperse (PDI > 0.5) (Fig. 3B). Instability of endogenous nano-vesicles was exacerbated in the presence of 10% FBS, causing sonicated lysate to aggregate within just one week (Fig. 3B).

To address potential aggregation of native cellular membrane vesicles and to promote draining of these vesicles to local LNs upon subcutaneous (s.c.) administration *in vivo,* we introduced a polyethylene glycol (PEG) layer on these cell membrane vesicles (Fig. 1) [31]. First, sonicated lysate containing membrane vesicles was incubated at 37 °C with calcium to promote membrane fusion and aggregation, which allowed for facile collection of membrane vesicles via simple table-top centrifugation. Washed particles were then mildly sonicated together in the presence of lipid-conjugated PEG (DSPE-PEG) and EDTA to chelate any remaining calcium. Upon desalting column purification, the resulting PEGylated cell membrane particles (PEG-NPs) exhibited an average hydrodynamic diameter of 130 ± 3 nm, PDI of 0.20 ± 0.02, and zeta potential of −39 mV ± 2 mV (Fig. 3A).

In sharp contrast to the gradual aggregation of endogenous membrane vesicles during long-term storage as shown above (Fig. 3B), the size of PEG-NPs stored at 4 °C in PBS or 10% FBS-containing PBS was maintained at ~130 nm with the PDI remaining below 0.25 for the course of four weeks. Importantly, when we incubated each formulation at 37 °C to better simulate *in vivo* conditions, differences in stability became apparent. Sonicated nano-vesicles (without PEGylation) rapidly aggregated within 1 day at 37 °C in either PBS or 10% FBS-PBS, whereas PEG-NPs maintained their size and monodispersity for at least 3 days (Fig. 3C). Overall, PEG-NPs outperformed the other lysate preparations during the simulated stability testing as shown by complete lack of aggregation. These results suggested that PEG-NPs may drain efficiently to local LNs following administration [31], whereas other lysate formulations may aggregate or be taken up by local cells *in vivo*, potentially limiting their draining to LNs upon s.c. administration.

3.3. In vitro T cell activation

We next tested the impact of various cell lysate formulations on cross-presentation of antigens by DCs and cross-priming of antigen-specific T cells *in vitro*. We pulsed BMDCs with lysate formulations for 1 day and performed T cell expansion assay with OT-I CD8α+ T cells. Media and OT-I peptide (sequence = SIINFEKL) served as negative and positive controls, respectively. Overall, stimulation of DCs with CpG, a potent TLR9 agonist composed of a single stranded DNA containing unmethylated CG motifs, was more effective at expansion of OT-I CD8α+ T cells compared with the use of MPLA (Supplementary Fig. 1). Based on these results, we chose to use CpG as the adjuvant for the remainder of our experiments.

BMDCs pulsed with PEG-NPs effectively induced T cell activation and proliferation, as evidenced by extensive dilution of the CFSE dye within the surviving T cells (Fig. 4A and B). CFSE dilution induced by the PEG-NPs *in vitro* was on par with the membrane fraction but more effective than FT lysate ($P < 0.0001$, Fig. 4A and B). The proliferation index, which reports the average number of divisions that proliferating cells undergo [32], was significantly higher for the PEG-NP group compared with FT lysate, cytosolic, or membrane fractions ($P < 0.001$, Fig. 4C). Additionally, we enumerated the overall number of T cells at the end of the experiments, as these data provide context to the CFSE dilution results. The number of live T cells remaining at the end of 3 day co-culture was at least two-fold greater for the PEG-NP group compared with the FT lysate or the membrane fraction group ($P < 0.001$, Fig. 4D). Notably, the PEG-NPs treatment sustained comparable number of live T cells as the SIINFEKL positive control group (Fig. 4D),

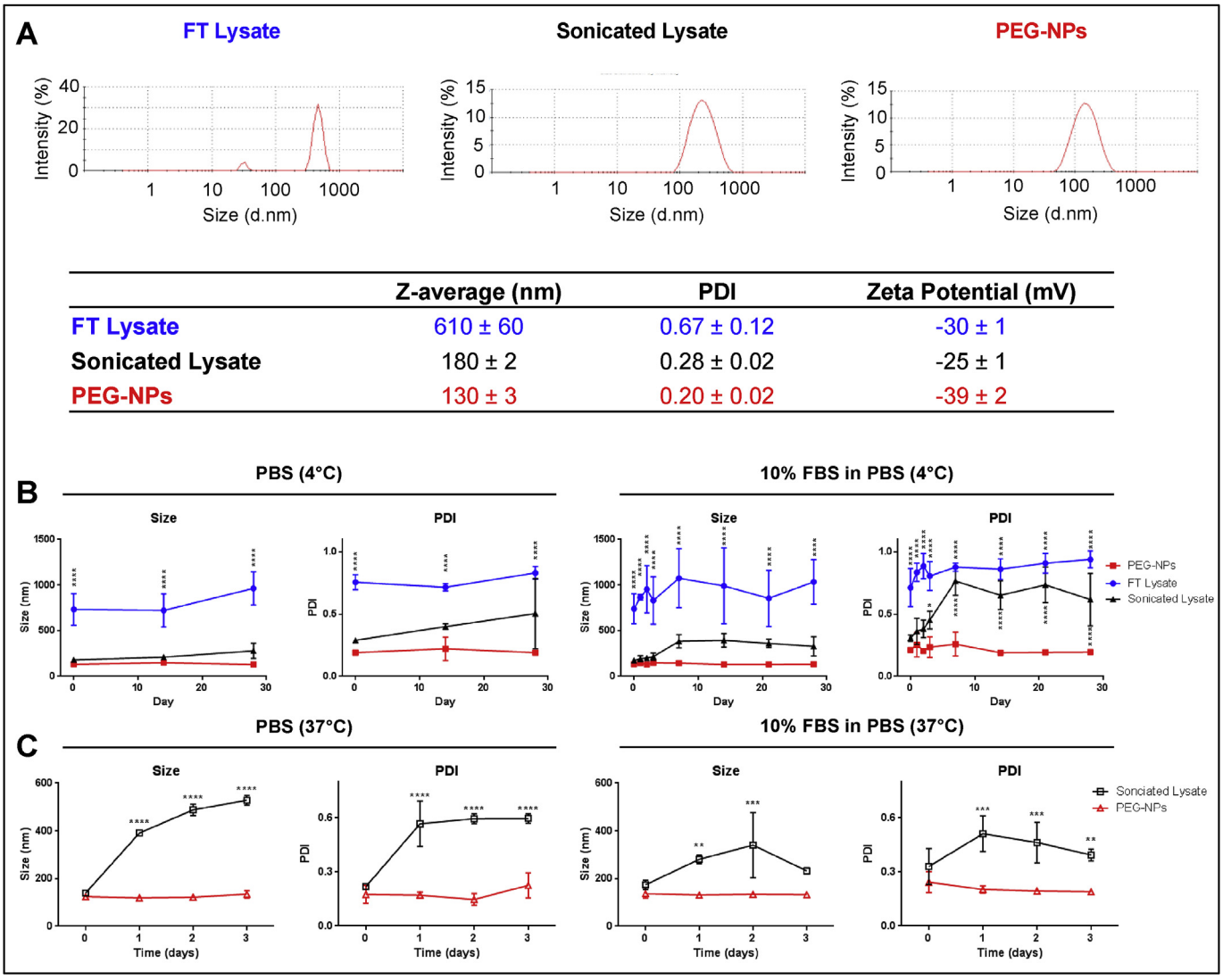

Fig. 3. Characterization of PEG-NPs. A. Particle size, PDI, and zeta potential were determined by dynamic light scattering analysis. **B.** Particles were incubated over a period of four weeks in PBS or 10%/90% FBS/PBS at 4 °C. Stability was assessed by determining particle sizes and PDIs over time. **C.** Particles were incubated over a period of three days in PBS or 10%/90% FBS/PBS at 37 °C. Aggregation was assessed by determining particle sizes and PDIs within the timeframe. Mean ± SD are shown. Statistical analysis was performed using two-way ANOVA comparison with Tukey's multiple comparison test (**$P < 0.01$, ***$P < 0.001$, ****$P < 0.0001$).

indicating strong induction and maintenance of T-cell proliferation supported by the PEG-NPs. Taken together, these results suggest that the PEG-NPs are taken up and processed effectively by DCs and lead to potent cross-priming of antigen-specific CD8α+ T cells.

3.4. Lymph node draining

PEGylation generally provides an advantage for subcutaneous administration of nano-formulations by promoting their trafficking to draining lymph nodes (dLNs) through drastically reducing interactions between the formulation and cells or serum proteins [33]. To determine the level of particle localization in dLNs at the whole tissue and cellular levels, lysate formulations were labeled with DiD, a lipophilic dye, and administered s.c. at the tail base. After 4, 24, and 48 h, inguinal dLNs were extracted, and the relative draining efficiency was assessed via whole LN imagining and flow cytometry. PEG-NPs exhibited significantly increased trafficking to dLNs and retention throughout 48 h, compared with FT lysate and unPEGylated NPs ($P < 0.0001$, Fig. 5A, Supplementary Fig. 2). We also examined APC populations that are responsible for lysate uptake. PEG-NPs were efficiently taken up by B cells, DCs, and F4/80 + macrophages *in vivo* (Fig. 5B–D), with B cells and DCs in particular exhibiting high lysate uptake even at 4 h time point. Interestingly, when we analyzed cellular uptake of these formulations *in vitro* using BMDCs, we found that PEG-NPs exhibited reduced cellular uptake, compared with sonicated lysate, FT lysate, and unPEGylated NP formulations (Supplementary Fig. 3), probably due to decreased association between PEGylated particle surface and cells. Although *in vitro* cellular uptake of PEG-NPs by DCs is not optimal, our results indicate that this *in vitro* condition does not fully reflect what happens *in vivo* and that PEG-NPs drain efficiently to dLNs and localize within APCs for potential antigen processing and presentation.

3.5. In vivo T cell activation and protective immunization

Next, we performed immunization study *in vivo* to examine T cell responses induced by FT lysate and PEG-NPs. We immunized C57BL/6 mice on days 0 and 14 with FT lysate or PEG-NPs containing 1 mg of total protein and 15 μg of CpG per mouse (Fig. 6A). One week post-prime, we examined peripheral blood mononuclear cells (PBMCs) for OVA-specific CD8α+ T cell responses via tetramer staining. We observed that immunization with PEG-NPs increased the frequency of OVA-specific CD8α+ T cells by 5-fold compared with FT lysate group

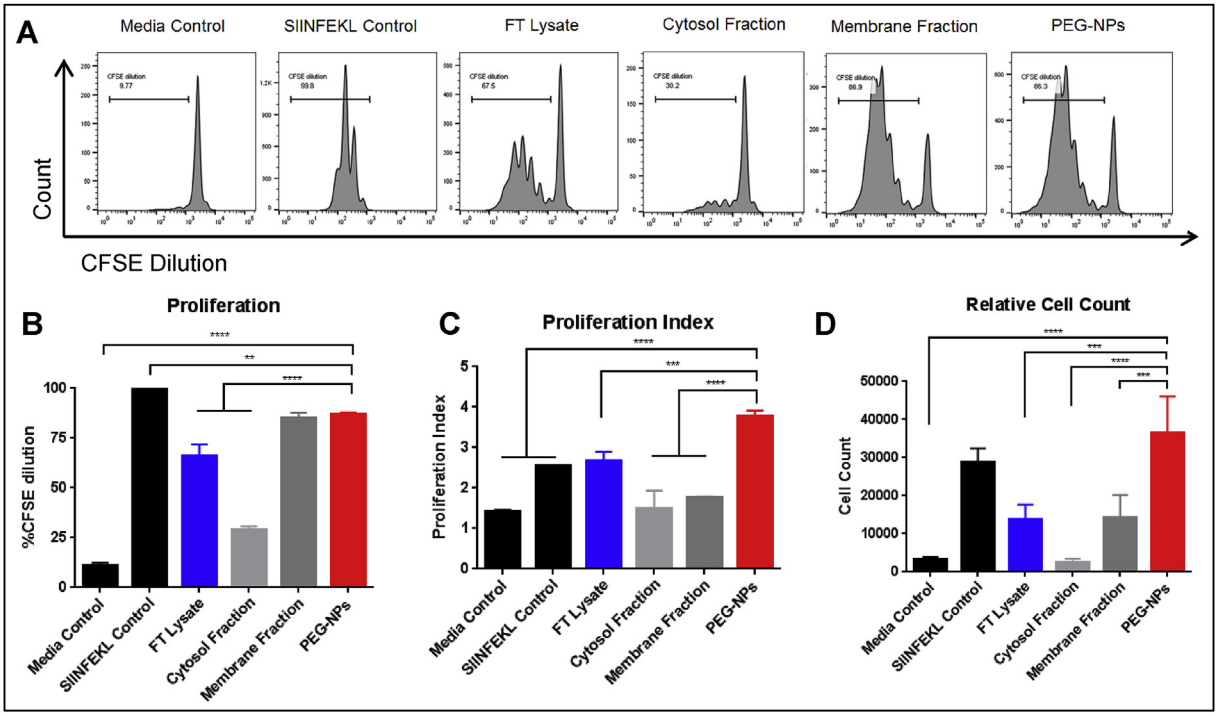

Fig. 4. Proliferation of antigen-specific CD8$^+$ T cells *in vitro*. Dendritic cells were pulsed with controls or lysate formulations overnight and then co-cultured with CFSE-labeled OT-I T cells for three days. **A.** Representative FACS histograms demonstrating CFSE dilution within proliferating OT-I T cells are shown. **B.** Average percentages of proliferated T cells after three days of culture are shown. **C.** Proliferation index was determined by FlowJo analysis software. **D.** The number of live CD8$^+$ T cells are shown. Mean ± SD are shown. Statistical analysis was performed using one-way ANOVA comparison with Tukey's multiple comparison test (**$P < 0.01$, ***$P < 0.001$, ****$P < 0.0001$).

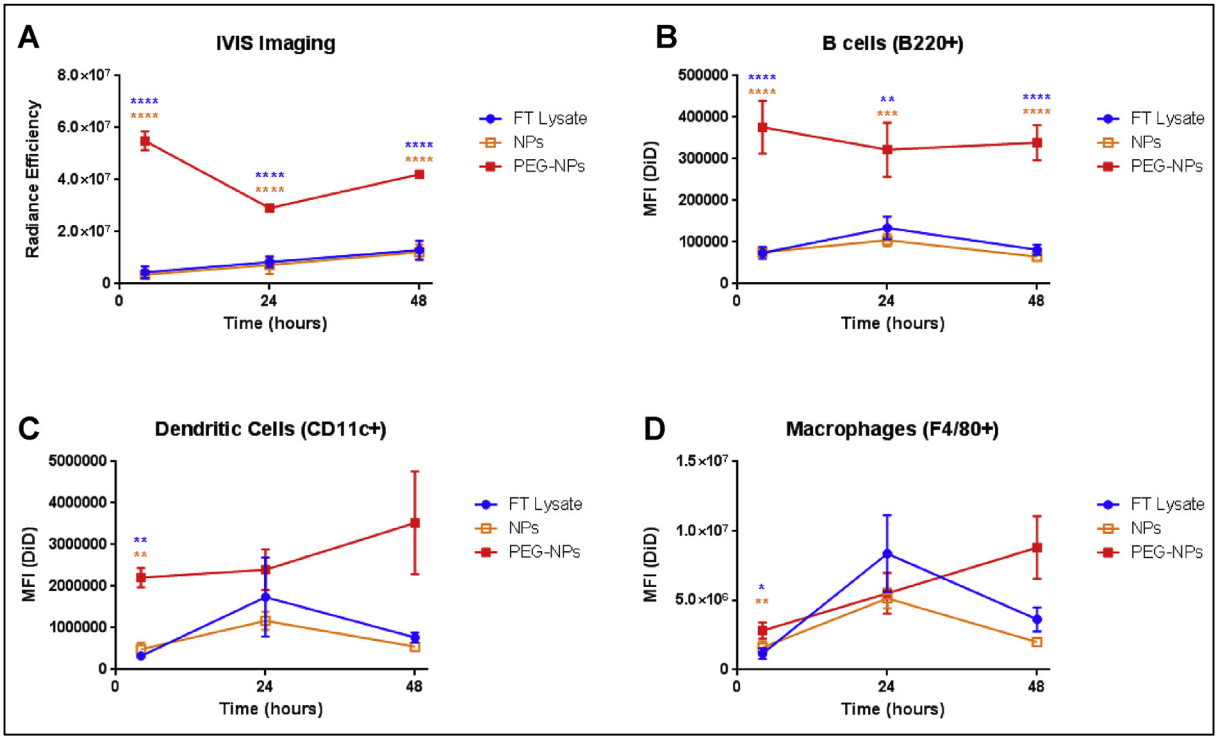

Fig. 5. *In vivo* lymph node draining. Cell lysate formulations were labeled with DiD fluorescent lipophilic dye and administered subcutaneously at tail base. **A.** 4, 24, and 48 h after injections, inguinal LNs were harvested and radiance efficiency measured by IVIS. **B-D.** Harvested LNs were dissociated into single cell suspensions and analyzed for DiD uptake by B cells, dendritic cells, and macrophages via flow cytometry. Mean ± SEM values are shown. Statistical analysis was performed using two-way ANOVA comparison with Tukey's multiple comparison test (*$P < 0.05$, **$P < 0.01$, ***$P < 0.001$, ****$P < 0.0001$).

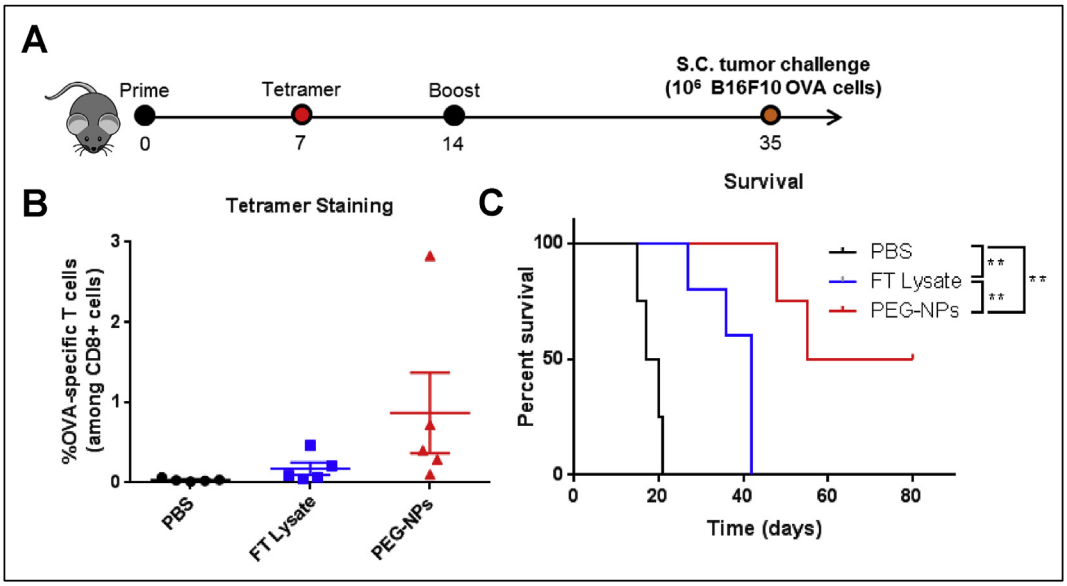

Fig. 6. Prophylactic immunization against B16F10 OVA tumor growth. A. Mice were immunized on day 0 and 14, followed by inoculation with 10^6 B16F10 OVA cells on day 35. **B.** OVA-specific $CD8^+$ T cell population among PBMCs was determined via tetramer staining. **C.** Overall survival following the tumor cell challenge on day 35 is shown. Mean ± SEM values are shown. Statistical analysis was performed using Log-rank (Mentel-Cox) test (**$P < 0.01$).

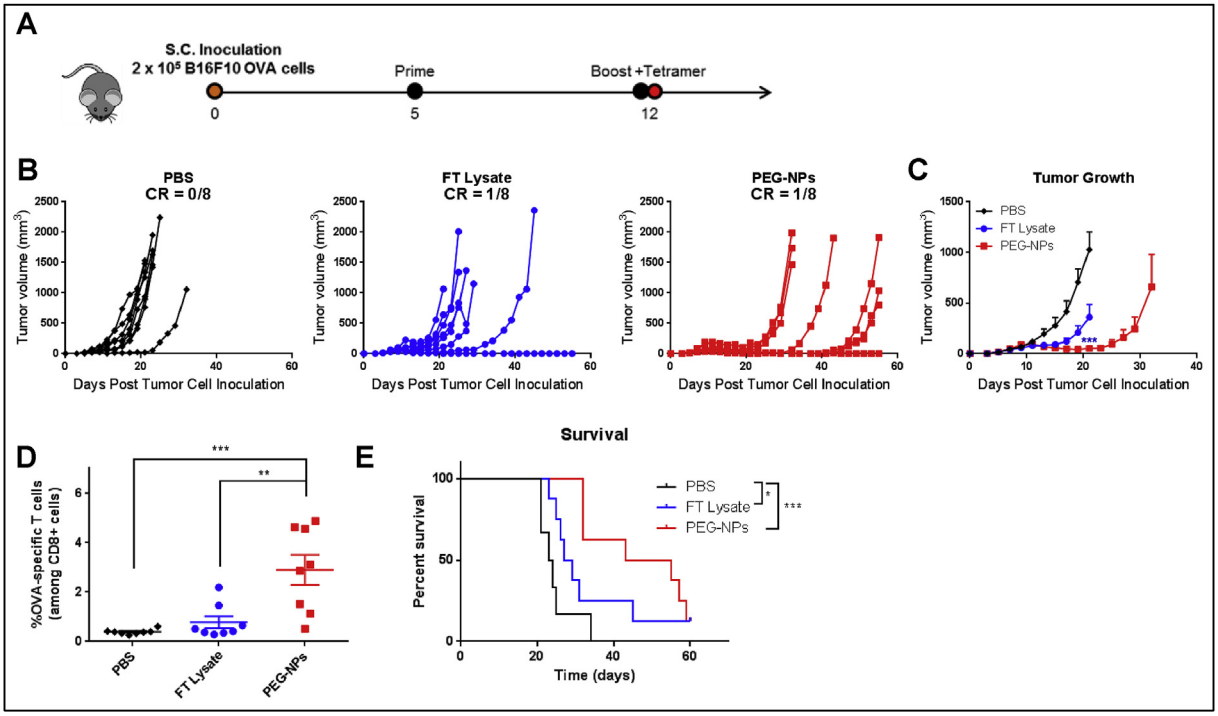

Fig. 7. Therapeutic treatment in B16F10 OVA tumor-bearing mice. A. C57BL/6 mice were inoculated with B16F10 OVA cells s.c. in the flank on day 0 and immunized on days 5 and 12. **B–C.** Plots of individual and average tumor growth curves are shown. **D.** Tetramer staining analysis via flow cytometry was performed to determine OVA-specific CTL responses among PBMCs on day 12. **E.** Overall animal survival is shown. Mean ± SEM are shown for panels C and D. Statistical analysis was performed using (C) two-way ANOVA with Tukey's multiple comparisons test compared to FT Lysate (blue asterisks); (D) one-way ANOVA comparison with Tukey's multiple comparison test; and (E) Log-rank (Mentel-Cox) test (*$P < 0.05$, **$P < 0.01$, ***$P < 0.001$ and ****$P < 0.0001$). (For interpretation of the references to colour in this figure legend, the reader is referred to the Web version of this article.)

although this difference was not statistically significant (Fig. 6B). We then examined the efficacy of vaccine formulations to induce protective immune responses against tumor challenge. Pre-immunized mice were inoculated s.c. at the flank with 10^6 B16F10 OVA cells (10-fold more cells than necessary to establish tumors in naïve animals) (Fig. 6A). Mice vaccinated with FT lysate exhibited the median survival time of 42 days, compared with 17 days in the PBS control group (Fig. 6C). Importantly, vaccination with PEG-NPs significantly extended the median survival time to 55 days ($P < 0.01$ versus PBS or FT lysate, Fig. 6C), and 50% of the animals remained free of tumor for at least 80 days, demonstrating the potency of PEG-NPs to elicit protective immune responses against tumor cells.

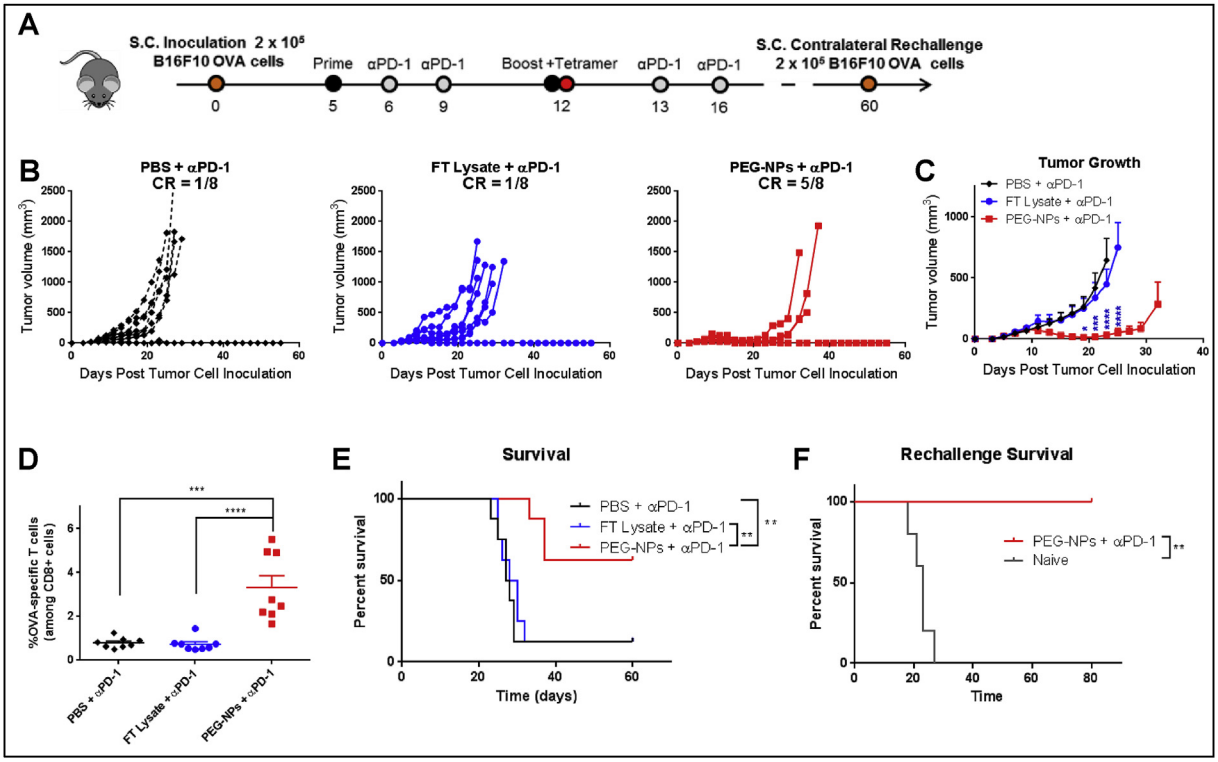

Fig. 8. Therapeutic vaccination plus *anti*-PD-1 immunotherapy in B16F10 OVA tumor-bearing mice. A. C57BL/6 mice were inoculated with B16F10 OVA cells s.c. in the flank on day 0 and treated with vaccines and *anti*-PD-1 therapy on indicated days. **B–C.** Tumor growth curves for individual mice and their average growth curves are shown. **D.** Tetramer staining analysis via flow cytometry was performed on day 12 to determine OVA-specific CTL responses among PBMCs. **E.** Overall survival is shown. **F.** Overall survival after mice were re-challenged with B16F10 OVA on day 60. Mean ± SEM are shown for panels C and D. Statistical analysis was performed using (C) two-way ANOVA with Tukey's multiple comparisons test compared to FT Lysate + αPD-1 (blue asterisks); (D) one-way ANOVA comparison with Tukey's multiple comparison test; and (E) Log-rank (Mentel-Cox) test (**$P < 0.01$, ***$P < 0.001$ and ****$P < 0.0001$). (For interpretation of the references to colour in this figure legend, the reader is referred to the Web version of this article.)

3.6. Therapeutic immunization

B16F10 OVA tumors were established via s.c. injection of 2×10^5 tumor cells at the right flank and once palpable tumors developed we vaccinated animals with either FT lysate or PEG-NPs on days 5 and 12 (Fig. 7A). Vaccination with FT lysate slowed tumor growth compared with PBS control ($P < 0.0001$ for days 19 and 21, Fig. 7B and C). Importantly, PEG-NPs treatment exerted significantly enhanced anti-tumor efficacy, further decreasing tumor growth, compared with the FT lysate group ($P < 0.001$ for day 21, Fig. 7B and C). Additionally, PEG-NPs treatment elicited robust antigen-specific CTL responses by day 12, characterized by 7.4-fold and 3.7-fold increases in the frequency of OVA-specific CD8α+ T cells among PBMCs, compared with PBS ($P < 0.001$) and FT lysate ($P < 0.01$) groups, respectively (Fig. 7D). These strong T-cell responses induced by PEG-NPs translated to increased animal survival, as mice treated with PEG-NPs exhibited the median survival of 55 days, compared with 22 and 27 days for PBS ($P < 0.001$) and FT lysate groups ($P = 0.12$), respectively (Fig. 7E). Notably, antigen-specific CD8α+ T cell responses induced by PEG-NPs in these tumor-bearing animals (Fig. 7D) was greater, compared with non-tumor bearing animals post PEG-NPs treatments (Fig. 6B), suggesting that the presence of antigen-expressing tumors may have boosted the effects of vaccination.

3.7. Combination therapy approach with immune checkpoint blockade

An immunosuppressive tumor microenvironment is currently a major challenge in allowing patients' endogenous immune responses from controlling cancer. Blocking the interaction between PD-1 and PD-L1, primarily expressed on T lymphocytes and tumor cells, respectively, allows T cells to engage and kill cancer cells, as demonstrated by the recent success of immune checkpoint inhibitors in the clinic [34]. Here, we aimed to further amplify T cell responses induced by PEG-NPs with co-administration of αPD-1 antibody, an immune checkpoint inhibitor, based on its clinical success [2,3] as well as our own observation that tumor-infiltrating lymphocytes, especially tumor antigen-specific T cells, had increased expression of PD-1 (Supplementary Fig. 4). Briefly, mice were inoculated s.c. at the right flank with 2×10^5 B16F10 OVA tumor cells and administered with PEG-NPs or FT lysate on days 5 and 12 together with intraperitoneal administration of αPD-1 IgG (100 μg per mouse per dose) on days 1 and 4 after each immunization (Fig. 8A). Tumor-bearing mice treated with FT lysate + αPD-1 IgG therapy exhibited similar tumor growth rates and median survival as animals treated with the αPD-1 IgG monotherapy (Fig. 8B and C), indicating the aggressive and poorly immunogenic nature of B16F10 OVA tumors. In sharp contrast, the combination of PEG-NPs + αPD-1 IgG therapy markedly decreased tumor growth, compared with αPD-1 monotherapy or FT lysate + αPD-1 treatment ($P < 0.0001$, day 23, Fig. 8B and C). Analysis of T cell responses in peripheral blood indicated that the PEG-NPs + αPD-1 IgG combination therapy induced 4.2-fold higher frequency of OVA-specific CD8α+ T cell responses, compared with the FT lysate + αPD-1 treatment group ($P < 0.0001$, Fig. 8D). Overall, the PEG-NPs + αPD-1 IgG combination therapy resulted in complete eradication of tumors in 63% of animals without reaching the median survival for the whole duration of the study. In contrast, animals treated with FT lysate + αPD-1 IgG exhibited only 13% response rate with the median survival of 28 days ($P < 0.01$, Fig. 8E).

We next determined if immune responses induced by the original treatment regimen established long-term systemic immunity against tumor recurrence. The survivors from the previous study (on day 60 of

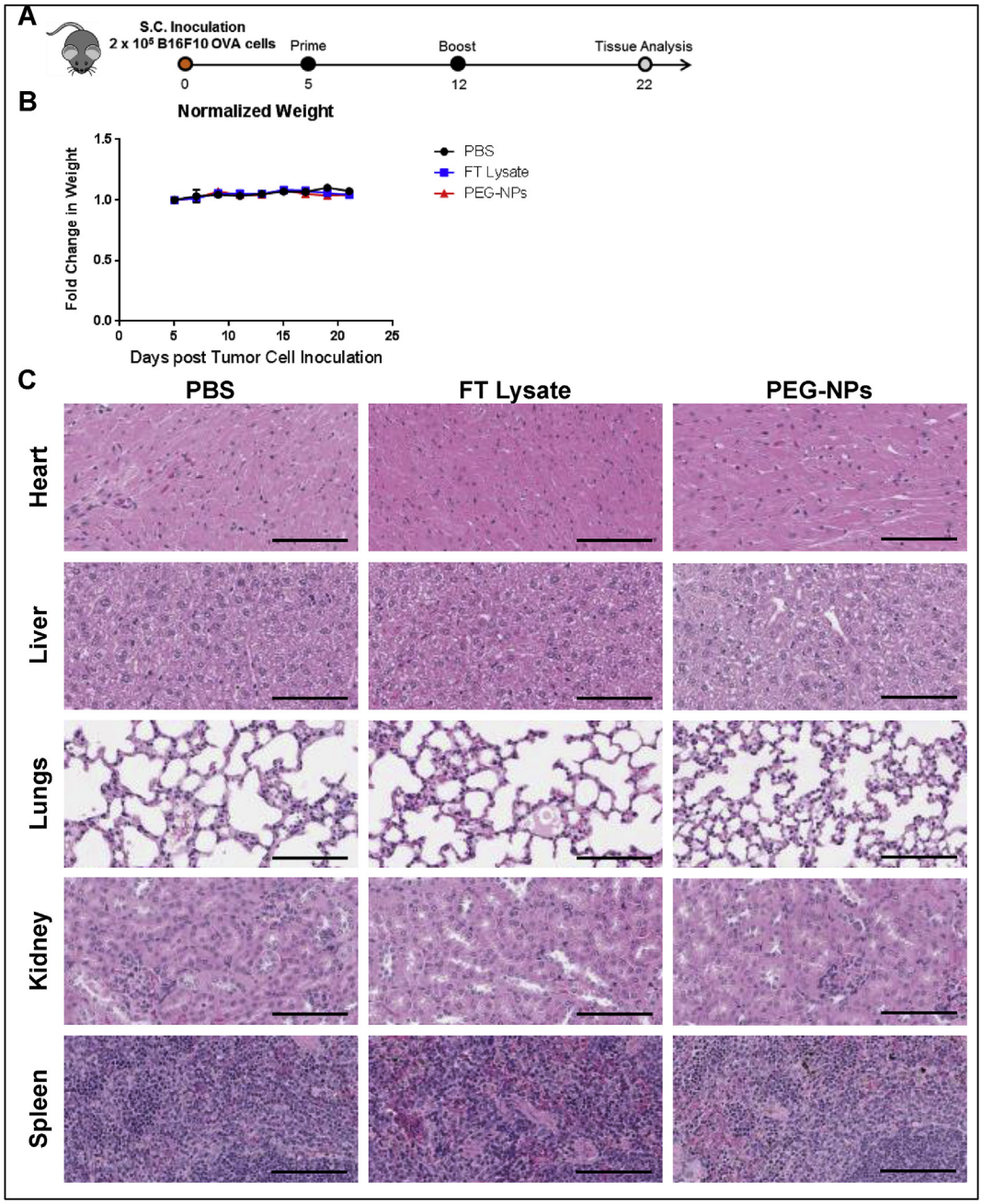

Fig. 9. Safety profiles of PEG-NPs. A. C57BL/6 mice were inoculated with B16F10 OVA cells on day 0 and immunized on days 5 and 12. **B.** Weight of the animals was measured starting on the day of first immunization. Mean ± SEM fold change is shown for each group. **C.** Representative H&E staining images of major organs harvested on day 22 are shown. Scale bars = 100 μm.

the original study) along with naïve control animals were inoculated with 2×10^5 B16F10 OVA tumor cells at the contralateral s.c. flank. None of the re-challenged survivors developed tumors for 80 days, whereas all naïve animals succumbed to tumor growth with the median survival of 23 days ($P < 0.01$, Fig. 8F). These results demonstrated that the PEG-NPs + αPD-1 IgG combination therapy elicited long-term protective immunity against the tumor cells.

3.8. Safety and toxicity

Cancer immunotherapy has always raised concerns regarding toxicity and potential autoimmune reactions, but most treatments up to date had been proven safe. In order to test the safety of our approach, we inoculated mice with B16F10 OVA cells and administered FT lysate or PEG-NPs on days 5 and 12 (Fig. 9A). Throughout the study, we observed no changes in animal health following administration of our vaccines, as demonstrated by normal behavior and maintained body weight (Fig. 9B). On day 22, mice were euthanized and major organs were harvested, fixed in neutral buffered formalin, processed, and stained with H&E. While minor skin inflammation and immune cell infiltrates, indicative of immune activation, were observed in the local sites of vaccination in animals treated with FT lysate or PEG-NPs, no systemic toxicity was observed in the heart, lungs, liver, spleen, or kidneys (Fig. 9C, Supplementary Fig. 5).

4. Conclusions

We have demonstrated that endogenous plasma membrane in

cancer cell lysate can be engineered into PEGylated nanoparticles with serum-stability and efficient lymph node draining. This cancer nano-vaccine platform can elicit strong CTL responses with potent anti-tumor efficacy, especially in combination with immune checkpoint blockade, resulting in complete regression of tumors in 63% of the animals and long-term immunity against tumor cell re-challenge. These studies show the promise of the nano-vaccine platform derived from whole tumor cell lysate as the basis for cancer vaccination.

Author contributions

L.J.O. and J.J.M. designed the study. L.J.O performed the experiments. J.D.B. C.P. and Y.X. assisted with animal experiments. R.K. contributed key reagents. L.J.O. and J.J.M. interpreted the data and wrote the paper.

Competing interests

The authors declare that they have no competing interests.

Acknowledgements

This work was supported in part by NIH (R01EB022563 and R01CA210273), MTRAC for Life Sciences Hub, UM Forbes Institute for Cancer Discovery Pilot Grant, and Emerald Foundation. J.J.M. is a Young Investigator supported by the Melanoma Research Alliance (348774), DoD/CDMRP Peer Reviewed Cancer Research Program (W81XWH-16-1-0369), and NSF CAREER Award (1553831). L.J.O. is supported by pre-doctoral fellowships from UM Rackham and AFPE. C.P. is supported by NIH/NIDCR Tissue Engineering and Regeneration Training Grant (DE007057). We acknowledge the NIH Tetramer Core Facility (contract HHSN272201300006C) for provision of MHC-I tetramers. Opinions interpretations, conclusions, and recommendations are those of the author and are not necessarily endorsed by the Department of Defense.

Appendix A. Supplementary data

Supplementary data related to this article can be found at https://doi.org/10.1016/j.biomaterials.2018.08.016.

References

[1] R.L. Siegel, K.D. Miller, A. Jemal, Cancer statistics, CA Cancer J. Clin. 68 (2018) (2018) 7–30.
[2] D.M. Pardoll, The blockade of immune checkpoints in cancer immunotherapy, Nat. Rev. Canc. 12 (2012) 252–264.
[3] S.L. Topalian, F.S. Hodi, J.R. Brahmer, S.N. Gettinger, D.C. Smith, D.F. McDermott, J.D. Powderly, R.D. Carvajal, J.A. Sosman, M.B. Atkins, P.D. Leming, D.R. Spigel, S.J. Antonia, L. Horn, C.G. Drake, D.M. Pardoll, L.P. Chen, W.H. Sharfman, R.A. Anders, J.M. Taube, T.L. McMiller, H.Y. Xu, A.J. Korman, M. Jure-Kunkel, S. Agrawal, D. McDonald, G.D. Kollia, A. Gupta, J.M. Wigginton, M. Sznol, Safety, activity, and immune correlates of anti-PD-1 antibody in cancer, N. Engl. J. Med. 366 (2012) 2443–2454.
[4] J.D. Wolchok, H. Kluger, M.K. Callahan, M.A. Postow, N.A. Rizvi, A.M. Lesokhin, N.H. Segal, C.E. Ariyan, R.A. Gordon, K. Reed, M.M. Burke, A. Caldwell, S.A. Kronenberg, B.U. Agunwamba, X.L. Zhang, I. Lowy, H.D. Inzunza, W. Feely, C.E. Horak, Q. Hong, A.J. Korman, J.M. Wigginton, A. Gupta, M. Sznol, Nivolumab plus ipilimumab in advanced melanoma, N. Engl. J. Med. 369 (2013) 122–133.
[5] R.O. Dillman, An update on the relevance of vaccine research for the treatment of metastatic melanoma, Melanoma Manag. 4 (2017) 203–215.
[6] M. Sznol, L.P. Chen, Antagonist antibodies to PD-1 and B7-H1 (PD-L1) in the treatment of advanced human cancer, Clin. Canc. Res. 19 (2013) 1021–1034.
[7] T.N. Schumacher, R.D. Schreiber, Neoantigens in cancer immunotherapy, Science 348 (2015) 69–74.
[8] M.M. Gubin, M.N. Artyomov, E.R. Mardis, R.D. Schreiber, Tumor neoantigens: building a framework for personalized cancer immunotherapy, J. Clin. Invest. 125 (2015) 3413–3421.
[9] U. Sahin, E. Derhovanessian, M. Miller, B.P. Kloke, P. Simon, M. Lower, V. Bukur, A.D. Tadmor, U. Luxemburger, B. Schrors, T. Omokoko, M. Vormehr, C. Albrecht, A. Paruzynski, A.N. Kuhn, J. Buck, S. Heesch, H. Katharina, F. Muller, I. Ortseifer, I. Vogler, E. Godehardt, S. Attig, R. Rae, A. Breitkreuz, C. Tolliver, M. Suchan, G. Martic, A. Hohberger, P. Sorn, J. Diekmann, J. Ciesla, O. Waksmann, A.K. Burck, M. Witt, M. Zillgen, A. Rothermel, B. Kasemann, D. Langer, S. Bolte, M. Diken, S. Kreiter, R. Nemecek, C. Gebhardt, S. Grabbe, C. Holler, J. Utikal, C. Huber, C. Loquai, O. Tureci, Personalized RNA mutanome vaccines mobilize poly-specific therapeutic immunity against cancer, Nature 547 (2017) 222–226.
[10] P.A. Ott, Z.T. Hu, D.B. Keskin, S.A. Shukla, J. Sun, D.J. Bozym, W.D. Zhang, A. Luoma, A. Giobbie-Hurder, L. Peter, C. Chen, O. Olive, T.A. Carter, S.Q. Li, D.J. Lieb, T. Eisenhaure, E. Gjini, J. Stevens, W.J. Lane, I. Javeri, K. Nellaiappan, A.M. Salazar, H. Daley, M. Seaman, E.I. Buchbinder, C.H. Yoon, M. Harden, N. Lennon, S. Gabriel, S.J. Rodig, D.H. Barouch, J.C. Aster, G. Getz, K. Wucherpfennig, D. Neuberg, J. Ritz, E.S. Lander, E.F. Fritsch, N. Hacohen, C.J. Wu, An immunogenic personal neoantigen vaccine for patients with melanoma, Nature 547 (2017) 217–221.
[11] R. Kuai, L.J. Ochyl, K.S. Bahjat, A. Schwendeman, J.J. Moon, Designer vaccine nanodiscs for personalized cancer immunotherapy, Nat. Mater. 16 (2017) 489–496.
[12] R. Kuai, X. Sun, W. Yuan, Y. Xu, A. Schwendeman, J.J. Moon, Subcutaneous nanodisc vaccination with neoantigens for combination cancer immunotherapy, Bioconjugate Chem. 29 (2018) 771–775.
[13] F.E. Gonzalez, A. Gleisner, F. Falcon-Beas, F. Osorio, M.N. Lopez, F. Salazar-Onfray, Tumor cell lysates as immunogenic sources for cancer vaccine design, Hum. Vaccines Immunother. 10 (2014) 3261–3269.
[14] D. Berd, H.C. Maguire, P. Mccue, M.J. Mastrangelo, Treatment of metastatic melanoma with an autologous tumor-cell vaccine - clinical and immunological results in 64 patients, J. Clin. Oncol. 8 (1990) 1858–1867.
[15] V.K. Sondak, J.A. Sosman, Results of clinical trials with an allogeneic melanoma tumor cell lysate vaccine: Melacine, Semin. Canc. Biol. 13 (2003) 409–415.
[16] T.D. de Gruijl, A.J.M. van den Eertwegh, H.M. Pinedo, R.J. Scheper, Whole-cell cancer vaccination: from autologous to allogeneic tumor- and dendritic cell-based vaccines, Canc. Immunol. Immunother. 57 (2008) 1569–1577.
[17] J.S. Yu, G.T. Liu, H. Ying, W.H. Yong, K.L. Black, C.J. Wheeler, Vaccination with tumor lysate-pulsed dendritic cells elicits antigen-specific, cytotoxic T-cells in patients with malignant glioma, Canc. Res. 64 (2004) 4973–4979.
[18] J.H. Kim, Y. Lee, Y.-S. Bae, W.S. Kim, K. Kim, H.Y. Im, W.K. Kang, K. Park, H.Y. Choi, H.M. Lee, W.K. Kang, H. Lee, H. Doh, B.-M. Kim, C.Y. Kim, C. Jeon, C.W. Jung, Phase I/II study of immunotherapy using autologous tumor lysate-pulsed dendritic cells in patients with metastatic renal cell carcinoma, Clin. Immunol. 125 (2007) 257–267.
[19] A. Ribas, B. Comin-Anduix, B. Chmielowski, J. Jalil, P. de la Rocha, T.A. McCannel, M.T. Ochoa, E. Seja, A. Villanueva, D.K. Oseguera, B.R. Straatsma, A.J. Cochran, J.A. Glaspy, L. Hui, F.M. Marincola, E. Wang, J.S. Economou, J. Gomez-Navarro, Dendritic cell vaccination combined with CTLA4 blockade in patients with metastatic melanoma, Clin. Canc. Res. 15 (2009) 6267–6276.
[20] S. Hamdy, A. Haddadi, R.W. Hung, A. Lavasanifar, Targeting dendritic cells with nano-particulate PLGA cancer vaccine formulations, Adv. Drug Deliv. Rev. 63 (2011) 943–955.
[21] Y. Fan, J.J. Moon, Nanoparticle Drug Delivery Systems Designed to Improve Cancer Vaccines and Immunotherapy, Vaccines (Basel) vol. 3, (2015), pp. 662–685.
[22] X. Wei, M. Ying, D. Dehaini, Y. Su, A.V. Kroll, J. Zhou, W. Gao, R.H. Fang, S. Chien, L. Zhang, Nanoparticle functionalization with platelet membrane enables multifactored biological targeting and detection of atherosclerosis, ACS Nano 12 (2018) 109–116.
[23] X. Zhang, P. Angsantikul, M. Ying, J. Zhuang, Q. Zhang, X. Wei, Y. Jiang, Y. Zhang, D. Dehaini, M. Chen, Y. Chen, W. Gao, R.H. Fang, L. Zhang, Remote loading of small-molecule therapeutics into cholesterol-enriched cell-membrane-derived vesicles, Angew. Chem. 56 (2017) 14075–14079.
[24] J. Tang, D. Shen, T.G. Caranasos, Z. Wang, A.C. Vandergriff, T.A. Allen, M.T. Hensley, P.U. Dinh, J. Cores, T.S. Li, J. Zhang, Q. Kan, K. Cheng, Therapeutic microparticles functionalized with biomimetic cardiac stem cell membranes and secretome, Nat. Commun. 8 (2017) 13724.
[25] A.V. Kroll, R.H. Fang, Y. Jiang, J.R. Zhou, X.L. Wei, C.L. Yu, J. Gao, B.T. Luk, D. Dehaini, W.W. Gao, L.F. Zhang, Nanoparticulate delivery of cancer cell membrane elicits multiantigenic antitumor immunity, Adv. Mater. 29 (2017).
[26] A.S. Cheung, S.T. Koshy, A.G. Stafford, M.M.C. Bastings, D.J. Mooney, Adjuvant-loaded subcellular vesicles derived from disrupted cancer cells for cancer vaccination, Small 12 (2016) 2321–2333.
[27] M.B. Lutz, N. Kukutsch, A.L.J. Ogilvie, S. Rossner, F. Koch, N. Romani, G. Schuler, An advanced culture method for generating large quantities of highly pure dendritic cells from mouse bone marrow, J. Immunol. Meth. 223 (1999) 77–92.
[28] L.J. Ochyl, J.J. Moon, Whole-animal imaging and flow cytometric techniques for analysis of antigen-specific CD8+T cell responses after nanoparticle vaccination, J. Vis. Exp. 98 (2015) e52771.
[29] H.T. Khong, S.A. Rosenberg, Pre-existing immunity to tyrosinase-related protein (TRP)-2, a new TRP-2 isoform, and the NY-ESO-1 melanoma antigen in a patient with a dramatic response to immunotherapy, J. Immunol. 168 (2002) 951–956.
[30] A.C. Theos, S.T. Truschel, G. Raposo, M.S. Marks, The Silver locus product Pmel17/gp100/Silv/ME20: controversial in name and in function, Pigm. Cell Res. 18 (2005) 322–336.
[31] D.J. Irvine, M.C. Hanson, K. Rakhra, T. Tokatlian, Synthetic nanoparticles for vaccines and immunotherapy, Chem. Rev. 115 (2015) 11109–11146.
[32] M. Roederer, Interpretation of cellular proliferation data: avoid the panglossian, Cytom Part A 79A (2011) 95–101.
[33] H. Jiang, Q. Wang, X. Sun, Lymph node targeting strategies to improve vaccination efficacy, J. Contr. Release 267 (2017) 47–56.
[34] L.P. Chen, X. Han, Anti-PD-1/PD-L1 therapy of human cancer: past, present, and future, J. Clin. Invest. 125 (2015) 3384–3391.